Helical Coil Flow: a Case Study

Marco Cozzini*
Renewable Energies and Environmental Technologies (REET) Research Unit, Fondazione Bruno Kessler (FBK),
Via alla Cascata 56/C, I-38123 Povo (TN), Italy
*E-mail: cozzini@fbk.eu

Abstract: Stationary flow configurations in curved pipes constitute an important subject from both the theoretical and the practical point of view. A typical application concerns the calculation of secondary flow effects on the thermal efficiency of heat exchangers. Motivated by a similar problem, this paper investigates the flow patterns in a helical duct of non trivial cross section. The considered regime is essentially laminar. A particular attention is devoted to the investigation of Dean structures, i.e., the recirculation cells arising in the secondary flow. The effect of duct torsion is put in evidence by an explicit comparison with a toroidal geometry of identical cross-section.

Keywords: secondary flow, laminar regime, helical coil

1 Introduction

The study of stationary flow configurations in curved pipes is an interesting field whose rigorous investigation can be dated back at least to the beginning of the 20-th century, with the experimental works of Eustice [4] and the theoretical analysis of Dean [2, 3]. This topic is of primary interest in several practical applications, ranging from the designing of heat exchangers to the study of blood flow in veins. Along the years, several cross-sectional geometries (circular, elliptical, square, rectangular, triangular) and pipe paths (toroidal, spiral, helical) have been considered in different flow regimes (laminar, mixed, turbulent) and with different approaches (experimental, analytical, numerical). The interplay of centrifugal and pressure forces in the formation of secondary flow (i.e., the flow field perpendicular to the main flow direction) has been extensively studied (see Ref. [1] for a review). In a wide range of conditions, a typical pattern consisting of two counter-rotating recirculation cells in the transverse direction has been found. These are sometimes called "Dean vortices", though the vortex-like velocity profile is actually a small perturbation superimposed on the main axial flow. The presence and the number of these Dean structures can vary as a function of fluid-dynamic and geometrical parameters (Reynolds number Re, pipe path curvature κ and torsion τ, pipe cross section). For circular pipes (pipe radius a) and purely toroidal flow (torus radius R), in the approximation of small curvature ratio $\delta = a/R \ll 1$ the effects of these parameters only depend on a simple dimensionless combination, the so-called Dean number De, typically defined as $\mathrm{De} = \mathrm{Re}\sqrt{\delta}$. From the point of view of heat exchange applications, in the laminar regime the recirculation introduced by secondary flow yields a significant enhancement in the fluid-wall heat transfer coefficient with respect to the case of a straight pipe. For a precise evaluation of the heat transport properties it is then important to obtain an accurate description of the transverse velocity components.

In this work, the water flow in a helical coil of non trivial cross-section (see Fig. 1) is studied. Fluid-dynamic, cross section and helix parameters are fixed by practical reasons. The numerical results are compared with those found in the literature for standard cross sections in similar conditions. A toroidal configuration with the same cross section is also considered for comparison.

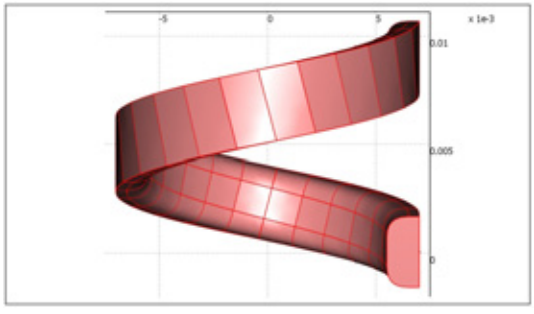

Figure 1. The considered helical coil channel.

The paper is organized as follows. Sec. 2 describes in details the considered system. The model implementation in Comsol Multiphysics is discussed in Sec. 3. The numerical results are presented in Sec. 4, for both the helical and the toroidal geometries. Conclusions are drawn in Sec. 5.

2 System description

This work arises from the analysis of an industrial application involving a heat exchanger based on a helical pipe. The water flowing in the channel is heated by a heat source placed on the helix axis. Due to the relatively small difference between the inlet and outlet cup mixing temperatures of the fluid, it is possible to assume purely incompressible flow. Hence, for a sufficiently large number of turns in the helical path, the velocity pattern in stationary conditions is basically constant at any channel cross section. In other words, finite size effects can be neglected and the system is well approximated by the infinite coil problem.

In an infinite helical coil channel, the velocity field and the pressure gradient clearly exhibit translation symmetry with respect to the arc-length coordinate of the helix. More explicitly, once expressed in the orthogonal curvilinear coordinates corresponding to the so called Frenet frame (defined by the tangent, normal, and binormal unit vectors), the velocity field and the pressure gradient are the same at any cross section. By a suitable coordinate transformation (see, e.g., Ref. [5]) it is therefore possible to reduce the original three-dimensional (3D) system to a purely two-dimensional (2D) problem on a generic channel cross section.

A less efficient implementation of the infinite coil problem relies on the full 3D Navier-Stokes equations under periodic-like boundary conditions. For example, it is possible to simulate a single helix turn by imposing exact periodicity to the velocity field and periodicity up to a constant (easily related to the desired pressure gradient) to the pressure field. Fractions of a single turn can be simulated by easily generalizing these constraints. This is the approach adopted in this paper, due to its direct connection (both in terms of model implementation and computational costs) with the finite size industrial system described above.

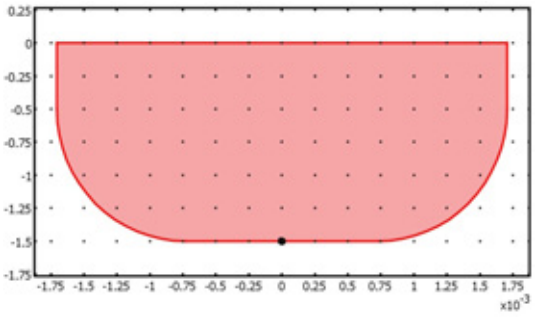

Figure 2. Duct cross section. The intersection of the helix curve described in the text with the cross section plane is marked by the thick point.

2.1 Geometry

The considered cross section is reported in Fig. 2. This shows the edges given by the channel walls in the plane orthogonal to the unit vector $\mathbf{t}$ tangent to the helix path. The hydraulic diameter $D_{\rm h}$ of the channel is

$$D_{\rm h} = 4A_{\rm ch}/P_{\rm ch} = 2.109 \text{ mm},$$

where $A_{\rm ch} = 4.66518$ mm^2 is the channel cross section area and $P_{\rm ch} = 8.847$ mm is the channel cross section perimeter. The helical duct coils around a cylinder of radius $R = 5.5$ mm. The helix at the inner side of the duct (passing through the point put in evidence in Fig. 2) is parametrized by

$$x(\phi) = R\cos\phi \ , \ y(\phi) = R\sin\phi \ , \ z = Z\phi/2\pi \ ,$$

where x, y, z are the cartesian coordinates of the helix position as a function of the azimuthal angle ϕ and $Z = 9$ mm is the helix pitch. The angle alpha between the tangent unit vector $\mathbf{t}$ and the x-y plane is given by

$$\tan\alpha = Z/2\pi R \ ,$$

while the curvature κ and the torsion τ of the curve are given by

$$\kappa = \frac{R}{R^2 + (Z/2\pi)^2} \ , \ \tau = \frac{Z/2\pi}{R^2 + (Z/2\pi)^2} \ .$$

In general, the fluid flow is affected by both the torsion and the curvature of the duct. To put in evidence the role of torsion, the helical duct is compared with a toroidal duct of identical cross section. The latter geometry is a mathematical abstraction which can be seen as the limit where the pitch Z tends to zero at fixed R. The toroidal geometry preserves the symmetry shown by the cross section, which is instead broken by the helical path. By exploting this symmetry, the study of the toroidal

path can then be made less computationally expensive than the helical one. The Reynolds number Re can be estimated by using the hydraulic diamter as

$$\mathrm{Re} = \rho \langle v \rangle D_\mathrm{h} / \eta \ ,$$

where $\langle v \rangle$ is the average velocity. The parameter δ, defined as the ratio between the channel radius and the curvature radius for circular ducts, can here be estimated by

$$\delta = D_\mathrm{h} \kappa / 2 \ .$$

3 Model implementation

The problem consists in the solution of the 3D Navier-Stokes equations in a toroidal and in a helical channel. The basic incompressible Navier-Stokes application mode of Comsol Multiphysics is used. Fluid is assumed to be water with constant density $\rho = 10^3$ kg/m^3 and viscosity $\eta = 10^{-3}$ Pa·s; gravity effects are neglected. No slip boundary conditions are used at the channel walls, while periodic-like boundary conditions are imposed at the inlet and outlet boundaries. As previously discussed, this corresponds to the infinite coil problem, where the velocity field and the pressure gradient have the same distribution at any channel cross section, independent of the arc-length coordinate. Pressure is then decreased by a given amount Δp between the inlet and the outlet boundaries and the problem is fully determined by specifying the pressure at a point.

The applied pressure gradients are approximately chosen to get average velocities between 0.1 m/s and 1 m/s, as in the industrial application motivating this work. This corresponds to Reynolds numbers ranging from about 200 to about 2000. As the curvature is $\kappa \sim 1/R$, the channel size to curvature ratio δ is of the order of 0.2 and the considered Dean numbers fall between 80 and 900.

Convergence is reached by keeping the defalut value of crosswind diffusion (0.1) in Comsol Multiphysics. Some isotropic diffusion has sometimes been used for intermediate simulations, in order to improve the initial condition for the final simulation without isotropic diffusion. The PARDISO solver has been used for all the considerd models. The Highly non linear problem option in Solver Parameters has revealed to be crucial in order to get convergence, though Manual tuning of damping paramters has often been used also. The choice of element order and the mesh quality effects on convergence are discussed in the next section.

4 Results

This section describes the obtained numerical results. The discussion starts with the toroidal geometry, where the analysis is simpler. Then the helical geometry is considered, where torsion effects play a non negligible role.

4.1 Toroidal path

In the toroidal geometry, due to the absence of torsion, the Dean number $\mathrm{De} = \mathrm{Re}\sqrt{\delta}$ is expected to completely characterize the flow. Due to the periodic-like boundary conditions, the arc-length for the simulation geometry can be chosen at will. Morover, the symmetry with respect to the plane orthogonal to the binormal unit vector $\mathbf{b}$ can be exploited to reduce model size. Two cases are considered here: a 10° arc-length geometry with half cross section and symmetry boundary conditions at the aforementioned plane, and a 90° arc-length geometry with full cross section. For a given average mesh element size, the 10° symmetric geometry can be clearly simulated at lower computational costs than the quarter turn geometry; on the other side, the latter geometry can be used to check the correctness of boundary conditions and the consistency of the symmetric model.

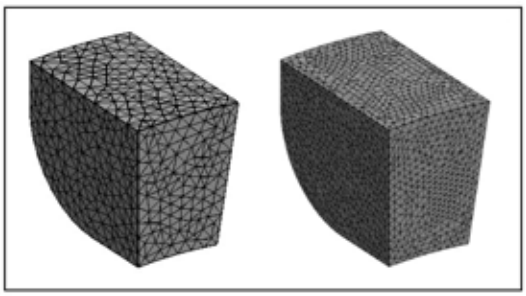

Figure 3. Meshes for the 10° symmetric toroidal geometry. Left: 9×10; right 16×18 (see text). Element order used in calculations: Lagrange - P_2P_1.

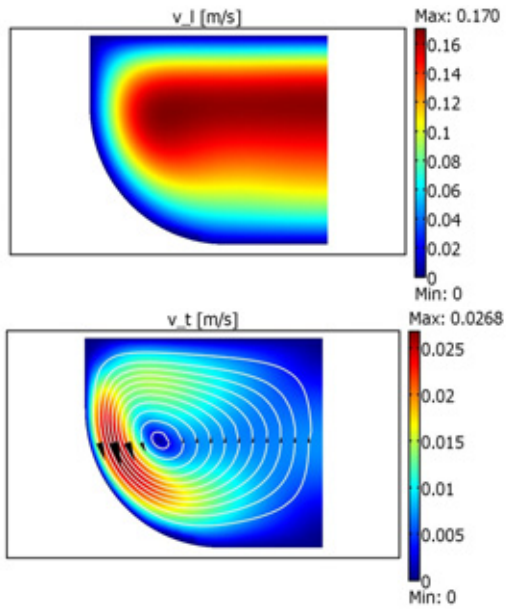

Figure 4. From top to bottom: main and secondary flow for a pressure gradient corresponding to 40 Pa / 360°. The simulation was performed in the 10° symmetric toroidal geometry with the 16×18 mesh (see Fig. 3). In the bottom panel, the secondary flow streamlines are visualized with proportional arrows indicating flow direction.

10° symmetric toroidal geometry. Calculations are performed on two different unstructured meshes of tetrahedral elements (see Fig. 3). For the first (second) mesh, the half cross section contains on average 9 (16) elements in the short direction (parallel to the normal unit vector $\mathbf{n}$ of the Frenet frame) and 10 (18) elements in the large direction (parallel to the binormal unit vector $\mathbf{b}$). Lagrange elements of second and first order have been chosen for the velocity and pressure variables, respectively (Lagrange - P_2P_1 in Comsol nomenclature). Periodic-like boundary conditions are easily implemented by the constraints

$$\begin{aligned} \mathbf{v}(\mathbf{r}_{out}) &= R_{\mathbf{b}}(\pi/18)\,\mathbf{v}(\mathbf{r}_{in})\ , \\ p(\mathbf{r}_{out}) &= p(\mathbf{r}_{in}) - \Delta p\ , \end{aligned}$$

where $R_{\mathbf{b}}(\pi/18)$ is the matrix yielding a 90° rotation around the axis given by the binormal unit vector $\mathbf{b}$, $\mathbf{r}_{out}$ is a generic point on the outlet boundary, and $\mathbf{r}_{in} = R_{\mathbf{b}}^{-1}(\pi/2)\,\mathbf{r}_{out}$ is the corresponding point at the inlet boundary. The problem is then completely specified by imposing the pressure value at a point, here chosen at the outlet boundary.

A pressure gradient corresponding to 40 Pa / 360° was studied in detail, in order to check the mesh accuracy. No significant difference in the results for the two meshes was observed (less than 0.5 % difference in secondary flow velocity). The results for the highest quality mesh are reported in Fig. 4. The main flow and the secondary flow velocities are $\mathbf{v}_l = (\mathbf{v}\cdot\mathbf{t})\mathbf{t}$ and $\mathbf{v}_t = (\mathbf{v}\cdot\mathbf{n})\mathbf{n}+(\mathbf{v}\cdot\mathbf{b})\mathbf{b}$, respectively. The average main flow velocity for the considered pressure gradient turns out to be $\langle v_l\rangle = 0.104$ m/s, corresponding to a Reynolds number Re $\simeq 220$. Since in the toroidal geometry one has $\delta = D_{\rm h}\kappa/2 \simeq 0.17$, the Dean number results De $=$ Re$\sqrt{\delta} \simeq 90$. This is a relatively small Dean number, where two Dean vortices are typically observed (both in elliptical and rectangular ducts). This is indeed the case also for the cross section considered in this paper. Note that the intensity of secondary flow is about 10 times smaller than that of main flow. As regards main flow, one can also observe that the position of the main flow velocity maximum is slightly shifted towards the outer wall with respect to the channel center, due to the centrifugal force.

Once verified that there is no significant difference between the results of the 9×10 and 16×18 meshes for the 40 Pa /360° case, further analysis of the toroidal geometry is performed with the lowest quality mesh in order to save compuational costs. The pressure drop is then progressively increased in order to study modifications in secondary flow. The flow rate dependence on the pressure drop is shown in Fig. 5. The resulting relation is approximately linear, corresponding to the laminar regime. The secondary flow dependence on the Dean number is also shown in Fig. 6.

Figure 6 shows the progressive deformation of the Dean vortex as the Dean number increases. The Dean structure is pushed towards the side walls of the duct and the secondary flow streamlines significantly deviate from the initial elliptical shape.

Quarter turn toroidal geometry. The geometry is drawn with an internal boundary on the symmetry plane, in order to reduce mesh asymmetry. Mesh symmetry is explicitly imposed at the inlet and outlet boundaries. Calculations are performed on an unstructured mesh of tetrahedral elements.

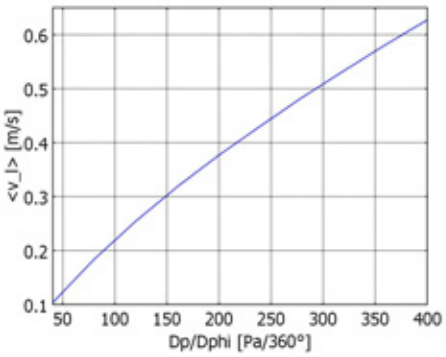

Figure 5. Mean flow average velocity as a function of pressure gradient in the 10° symmetric toroidal geometry.

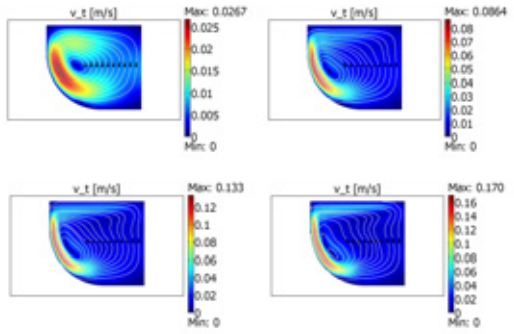

Figure 6. From left to right, top to bottom: secondary flow at 40, 160, 280, 400 Pa / 360° in the 10° symmetric toroidal geometry. The Dean numbers for the four cases are about 90, 276, 419, 543.

The results of this model are compared with those of the 9×10 mesh of the 10° symmetric geometry in order to check symmetry effects and possible dependences on the chosen arc-length. To this purpose, it is important to have a similar numerical precision in the two models. However, it was found to be difficult to get convergence with a 9×10 mesh (in terms of half section) in the quarter turn geometry. Therefore, a coarser mesh was chosen but with higher order Lagrange elements. In the chosen mesh (see Fig. 7), the duct cross section contains 4 elements in the direction of the normal unit vector **n** and 10 elements in the direction of the binormal unit vector **b** (for comparison with the 10° symmetric geometry, note that the half section mesh is then 4×5). Lagrange elements of third and second order are chosen for the velocity and pressure variables, respectively (Lagrange - P_3P_2 in Comsol nomenclature). Periodic-like boundary conditions are now implemented by the constraints $\mathbf{v}(\mathbf{r}_{out}) = R_{\mathbf{b}}(\pi/2)\,\mathbf{v}(\mathbf{r}_{in}), p(\mathbf{r}_{out}) = p(\mathbf{r}_{in}) - \Delta p$, with the same notation used before. Again, the problem is completely specified by imposing the pressure value at a point.

The chosen pressure gradient is given by 40 Pa / 360°. The resulting secondary flow is nearly identical to that found for the 10° symmetric geometry with the 9×10 mesh (compare Fig. 8 with upper left panel of Fig. 6).

4.2 Helical path

In the helical geometry, the presence of a finite torsion breaks the symmetry of the cross section, giving rise to a peculiar secondary flow which changes significantly the structure of Dean recirculation cells. The Dean number is now not sufficient to completely characterize the flow. On the other hand, the behaviour of the principal flow is not much affected by torsional effects.

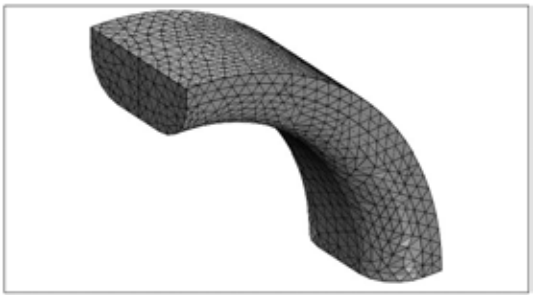

Figure 7. Mesh for the quarter turn toroidal geometry. Element order used in calculations: Lagrange - P_3P_2.

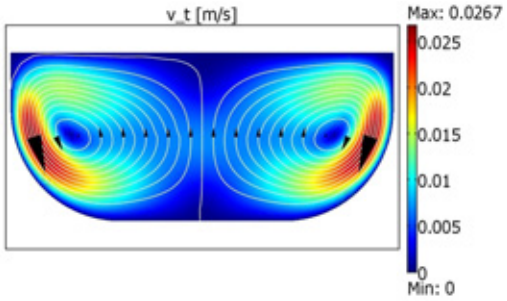

Figure 8. Secondary flow at 40 Pa / 360° in the quarter turn geometry of Fig. 7. Secondary flow streamlines with proportional arrows indicating the velocity direction are also plotted.

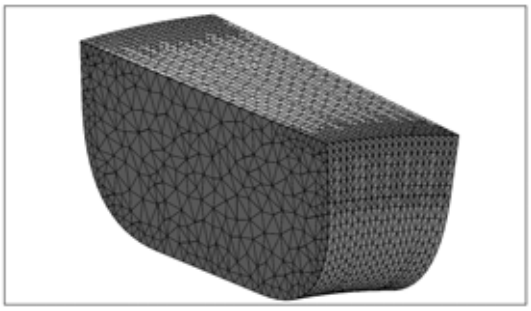

Figure 9. Mesh for the 10° helical geometry. Element order used in calculations: Lagrange - P_3P_2.

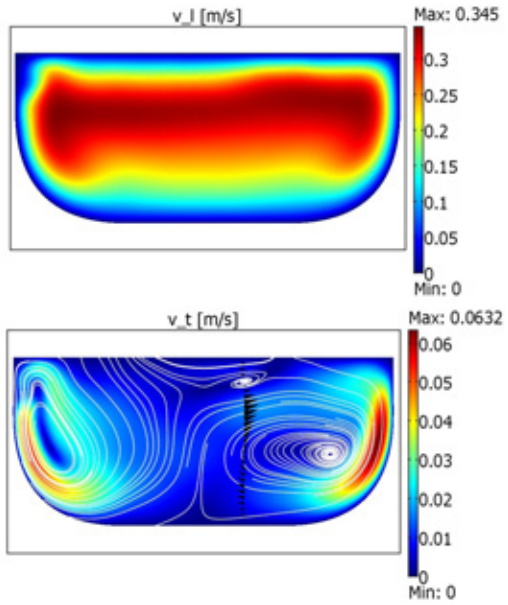

Figure 10. From top to bottom: main and secondary flow for a pressure gradient corresponding to 100 Pa / 360°. Mesh and element order as in Fig. 9. In the bottom panel, the secondary flow streamlines are visualized with proportional arrows indicating flow direction.

Similarly to the case of the toroidal geometry, two different arc-lengths are used to simulate the behaviour for the helical path: a 10° arc-length geometry, and a 360° arc-length (i.e., single turn) geometry (the angle is the azimuthal angle around the helix axis).

10° helical geometry. An unstructured mesh of tetrahedral elements (roughly corresponding to a 10×12 mesh with the half section notation used above) has been chosen (see Fig. 9). Lagrange elements of third and second order have been chosen for the velocity and pressure variables, respectively (Lagrange - P_3P_2 in Comsol nomenclature), making the precision of this simulation at least comparable to that of the best mesh in the 10° symmetric toroidal geometry. Periodic-like boundary conditions are implemented as

$$\begin{aligned} \mathbf{v}(\mathbf{r}_{out}) &= R_z(\pi/18)\,\mathbf{v}(\mathbf{r}_{in}) \ , \\ p(\mathbf{r}_{out}) &= p(\mathbf{r}_{in}) - \Delta p \ , \end{aligned}$$

where the only difference with respect to the toroidal geometry is that the rotation axis of the matrix $R_z(\pi/18)$ is now given by the helix axis (here pointing in the z direction) and no more by the binormal unit vector $\mathbf{b}$. Once more, the problem is completely specified by imposing the pressure value at a point (chosen at the outlet boundary).

A pressure gradient corresponding to 100 Pa / 360° is studied. The obtained results are shown in Fig. 10. The average main flow velocity turns out to be $\langle v_l \rangle = 0.215$ m/s, corresponding to a Reynolds number Re $\simeq 453$. In the helical geometry one has $\delta = D_{\rm h}\kappa/2 \simeq 0.16$, and the Dean number results De $= \mathrm{Re}\sqrt{\delta} \simeq 181$. The average intensity of secondary flow is about 10 times smaller than that of main flow.

With respect to the toroidal geometry, some differences are evident. The symmetry of the flow pattern is broken, more significantly in the secondary flow. Moreover, secondary flow shows the appearence of a small additional Dean structure, which was not observed in the toroidal geometry for similar Dean numbers. A remark is in order here. While in the toroidal case the Frenet normal and binormal vectors are oriented in the same way at every point of a given cross section, in the helical geometry this is not the case. It is therefore more difficult to obtain a plot of the secondary flow. As a resonable approximation, instead of using the exact secondary flow $\mathbf{v}_t = (\mathbf{v}\cdot\mathbf{n})\mathbf{n}+(\mathbf{v}\cdot\mathbf{b})\mathbf{b}$, where $\mathbf{n}$ and $\mathbf{b}$ vary even on the same cross section, a kind of average secondary flow was used, namely

$$\mathbf{v}_t = (\mathbf{v}\cdot\mathbf{n}_0)\mathbf{n}_0 + (\mathbf{v}\cdot\mathbf{b}_0)\mathbf{b}_0 \ ,$$

where $\mathbf{n}_0$ and $\mathbf{b}_0$ are calculated at the center of the considered cross section (so that the projection applied to the velocity field depend on the cross section, but not on the position on a given cross section). This slightly alters the streamline plots for the secondary flow; nevertheless, the additional small Dean structure observed here does not disappear for small variations in the secondary flow average

procedure, suggesting that this is not a spurious effect due to the chosen visualization.

Single turn helical geometry. Calculations are here performed on a structured mesh of prism elements (swept mesh with 96 element layers along the helical path). Boundary conditions are implemented as in the previous cases. The mesh is significantly coarser than the mesh for the 10° helical geometry (see Fig. 11); the results are nevertheless reasonably close (2% error in main flow, 10% error in secondary flow) to those of the best mesh. In particular, the numerical precision is sufficient to get reliable results for the dependence of the flow rate on the pressure drop, which is shown in Fig. 12 for pressure gradients between 100 and 1000 Pa / 360° (corresponding to Dean numbers up to 930). Though the relation between the average velocity and the pressure drop exhibits some deviation from linearity, the regime can still be considered laminar.

Qualitatively, it is possible to see that the symmetry breaking in the Dean flow becomes more and more evident as the pressure drop increases, giving rise to a slight growth of a Dean structure at the expenses of the other, as seen in the literature for helical flow. The mesh quality is however not satisfactory for a detailed investigation of secondary flow streamlines, which are hence not shown here.

5 Conclusion

In summary, this work studies the velocity field arising in a toroidal and in a helical coil channel with non standard cross section. Particular attention is devoted to the secondary flow velocity profile and to the relation between the mean velocity and the applied pressure drop. The flow regime is laminar (basically linear pressure-velocity relation).

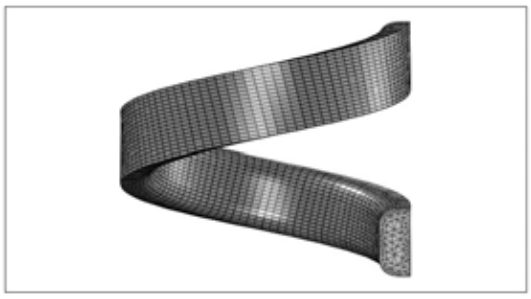

Figure 11. Mesh for the 360° helical path. Element order used in calculations: Lagrange - P_2P_1.

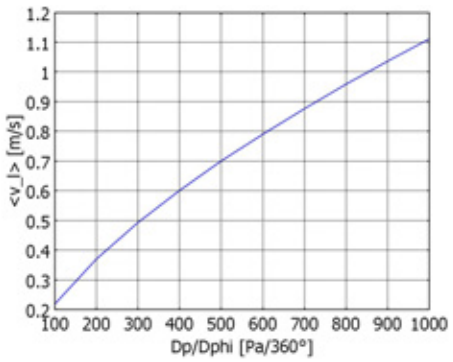

Figure 12. Average velocity as a function of pressure gradient in the single turn helix geometry. Mesh and element order as in Fig. 11.

The obtained results are relevant for the detailed understanding of heat exchange applications, where the knowledge of secondary flow provides usuful information which can be coupled with more empirical methods [6].

References

[1] S. A. Berger, L. Talbot, and L. S. Yao, *Flow in curved pipes*, Ann. Rev. Fluid Mech. **15** (1983), 461–512.

[2] W. R. Dean, *Note on the motion of fluid in a curved pipe*, Phil. Mag. **4** (1927), 208223.

[3] ———, *The streamline motion of fluid in a curved pipe*, Phil. Mag. **5** (1928), 673693.

[4] J. Eustice, *Flow of water in curved pipes*, Proc. R. Soc Lond. A **84** (1910), 107–119.

[5] T. J. Hüttl, C. Wagner, and R. Friedrich, *Navier-stokes solutions of laminar flows based on orthogonal helical coordinates*, Numerical methods in laminar and turbulent flow **10** (1997), 191–202.

[6] P. Naphon and S. Wongwises, *A review of the heat transfer and flow characteristics in the curved pipes*, Renew. Sustain. Energy Rev. **10** (2006), 463–490.

Acknowledgements

The author would like to thank Cesare Tozzo for useful discussions concerning Comsol Multiphysics.